Available online at www.sciencedirect.com
ScienceDirect
Journal of Power Sources 178 (2008) 723–728
JOURNAL OF POWER SOURCES
www.elsevier.com/locate/jpowsour

Short communication

The synthesis and lithium intercalation electrochemistry of VO_2(B) ultra-thin nanowires

Graham Armstrong [a], Jesús Canales [b], A. Robert Armstrong [a], Peter G. Bruce [a,*]

[a] *EaStCHEM, School of Chemistry, University of St. Andrews, Scotland, UK*
[b] *Renewable Energy Research Institute, Universidad de Castilla la Mancha, Paseo de la investigación 1, 02006 Albacete, Spain*

Received 7 November 2007; received in revised form 8 November 2007; accepted 9 November 2007
Available online 19 November 2007

Abstract

Ultra-thin (<10 nm diameter) VO_2(B) nanowires have been synthesised, characterised structurally and morphologically and their lithium intercalation electrochemistry investigated. The wires exist in bundles and exhibit significant preferred orientation. They have a capacity to intercalate lithium of 265 mAh g^{-1} ($Li_{0.82}VO_2$(B)) at a rate of 10 mA g^{-1} compared with thicker wires of 50–100 nm diameter which exhibit a capacity of 200 mAh g^{-1} at the same rate. The load curves, structure and morphology remain stable on cycling.

Keywords: Lithium-ion battery; Nanowires; Vanadium oxide; Cathode materials

1. Introduction

Nanomaterials are receiving increasing attention as electrodes and electrolytes for new generations of rechargeable lithium batteries delivering higher power and energy density [1–5]. Several nanostructures are being examined, including nanoparticles, mesoporous materials, nanoarchitectured surfaces, nanosheets, nanobelts, nanotubes and nanowires [6–13].

Recently, synthesis of the fifth polymorph of titanium dioxide, TiO_2(B), in the form of nanowires and nanotubes has been reported [14,15]. The properties of the TiO_2(B) nanowires and nanotubes as hosts for lithium intercalation have been examined and it has been shown that lithium can be intercalated up to a composition $Li_{0.98}TiO_2$(B), corresponding to a specific capacity of 330 mAh g^{-1}, with most of the capacity being delivered at a potential of 1.6 V versus Li^+(1 M)/Li [16–18].

Several polymorphs of vanadium dioxide are known including VO_2(R) with the rutile structure, VO_2(M) a monoclinically distorted rutile structure associated with a metal–insulator transition, VO_2(A) with a tetragonal structure and VO_2(B), which is isostructural with TiO_2(B) [19–21]. All the polymorphs have been prepared in the form of nanomaterials including VO_2(B) [22–32]. Previous reports of VO_2(B) nanowires have focused on materials in which the wire diameter is typically 50–200 nm. Here we describe the synthesis, structure, morphology and lithium intercalation electrochemistry of ultra-thin VO_2(B) nanowires (<10 nm). As far as we are aware only one previous report has mentioned VO_2 nanowires of comparable dimensions, no detailed structural characterisation and no electrochemistry were presented [28]. Although the focus of this paper will be on ultra-thin VO_2(B) nanowires, some results for thicker nanowires will be presented for comparison and to set the behaviour of the ultra-thin nanowires in context.

2. Experimental

Two different routes were employed for the synthesis of VO_2(B) nanowires, they were adapted from the ethylene glycol method reported by Chen et al. [28]. The preparation of standard nanowires involved mixing 10 ml ethylene glycol, 30 ml of distilled water and 0.6 g of V_2O_5 (Aldrich, 99.6+ %). The mixture was stirred for 1 h and the resulting suspension transferred to a 40 ml autoclave then heated at 180 °C for 48 h. The product was

* Corresponding author. Tel.: +44 1334 463825; fax: +44 1334 463808.
E-mail address: pgb1@st-andrews.ac.uk (P.G. Bruce).

0378-7753/$ – see front matter © 2007 Elsevier B.V. All rights reserved.
doi:10.1016/j.jpowsour.2007.11.028

filtered, washed with distilled water and ethanol, before drying overnight at 80 °C. Ultra-thin nanowires were prepared by mixing 10 ml of ethylene glycol, 10 ml of distilled water and 0.6 g of V_2O_5. After stirring for 1 h the resulting suspension was transferred to a 40 ml autoclave then heated at 150 °C for 3 h. The product was washed and dried as above. Small changes (±10%) in the volume of water, temperature and quantity of V_2O_5 used were found to have little or no effect on the resultant products.

Powder X-ray diffraction was performed using a Philips X'Pert system operating in Bragg–Brentano geometry and fitted with a secondary monochromator (Cu Kα, λ = 1.5418 Å). Transmission electron microscopy was performed on a Jeol JEM-2011 electron microscope operating at 200 kV and equipped with and Oxford-Link EDS detector and a Gatan 974 CCD camera for high-resolution imaging. Electrochemical properties were measured on electrodes prepared using mixtures comprising 75% active material, 18% Super S or Super P carbon and 7% Kynar Flex 2801 binder, dry mixed and pressed into pellets. Measurements were made using two-electrode coin cells comprising a VO_2(B) working electrode and Li metal counter electrode. Electrolytes used were a 1-m solution of $LiPF_6$ in propylene carbonate and 1 m lithium bis(oxalato)borate (LiBOB) in propylene carbonate. All cells were constructed and handled in an Ar filled MBraun glovebox. Electrochemical measurements were carried out at 30 °C using a Biologic MacPile II system or Maccor battery cycler.

3. Results and discussion

3.1. Structure and morphology

Transmission electron micrographs of ultra-thin (6–10 nm diameter) and standard nanowires (50–100 nm diameter) are shown in Fig. 1. The ultra-thin wires are arranged in bundles within which the wires lie in the same direction. In contrast, the standard wires are not so arranged but exist as isolated wires. The standard nanowires exhibit lengths of several microns whilst the ultra-thin wires are several hundred nanometers in length. Examination of many regions of the samples indicates that the morphologies and dimensions of the ultra-thin and standard nanowires are present throughout the respective materials. High-resolution transition electron micrographs for ultra-thin and standard VO_2(B) wires are shown in Fig. 2. Lattice spacings of 11.6 Å and 3.6 Å are highlighted in figures, which correspond closely to the *d*-spacings of the (1 0 0) and (0 1 0) reflections for VO_2(B). Examination of the Fourier transformed selected area electron diffraction patterns (shown as insets in Fig. 2) indicates that the nanowires are essentially single crystals. The [0 0 1] crystallographic direction is perpendicular to the long axis of the wires. In the case of the ultra-thin wires the appearance of additional "satellite" spots arises from the difficulty in avoiding the beam intercepting more than one wire in a bundle in the *z*-direction. This results in "twinned-like" SAED patterns.

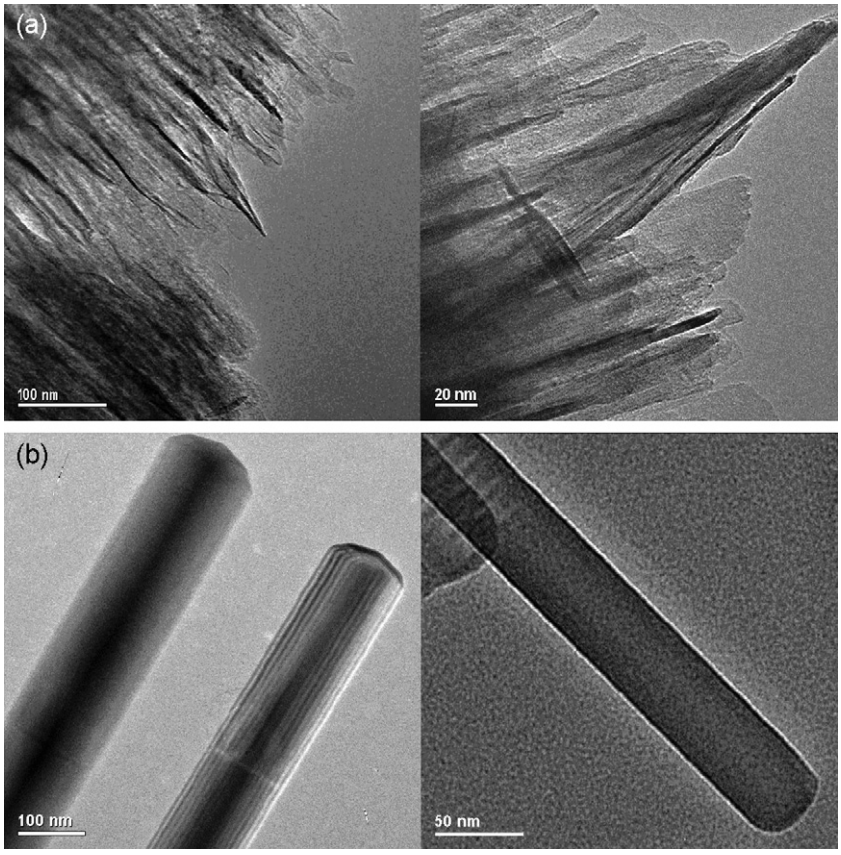

Fig. 1. TEM images of (a) ultra-thin VO_2(B) nanowires and (b) standard VO_2(B) nanowires.

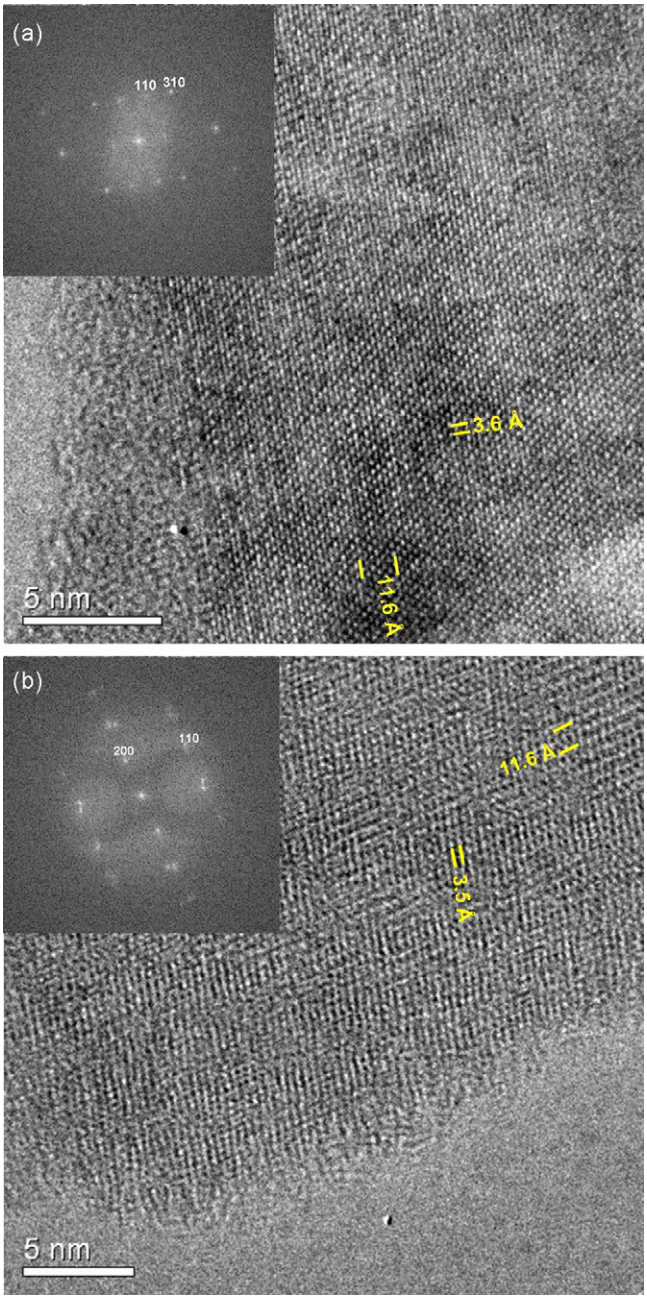

Fig. 2. HRTEM image and the corresponding FT SAED pattern of a VO_2(B) nanowire viewed down the [0 0 1] zone axis. (a) Standard nanowire and (b) ultra-thin nanowire.

Powder X-ray diffraction data for ultra-thin and standard nanowires are shown in Fig. 3a along with a simulated powder diffraction pattern based on the known crystal structure of VO_2(B). The crystal structure of VO_2(B) is shown in Fig. 3b and consists of sheets of edge sharing VO_6 octahedra linked by corner sharing to adjacent sheets along the *c*-direction of the unit cell [33]. The powder pattern for the standard wires agrees well with that generated for the crystal structure of VO_2(B), however this is not the case for the ultra-thin nanowires. Examination of the powder X-ray diffraction data for the ultra-thin wires reveals an interesting feature. Whereas several of the VO_2(B) peaks are present, a number are clearly absent. The absences correspond to

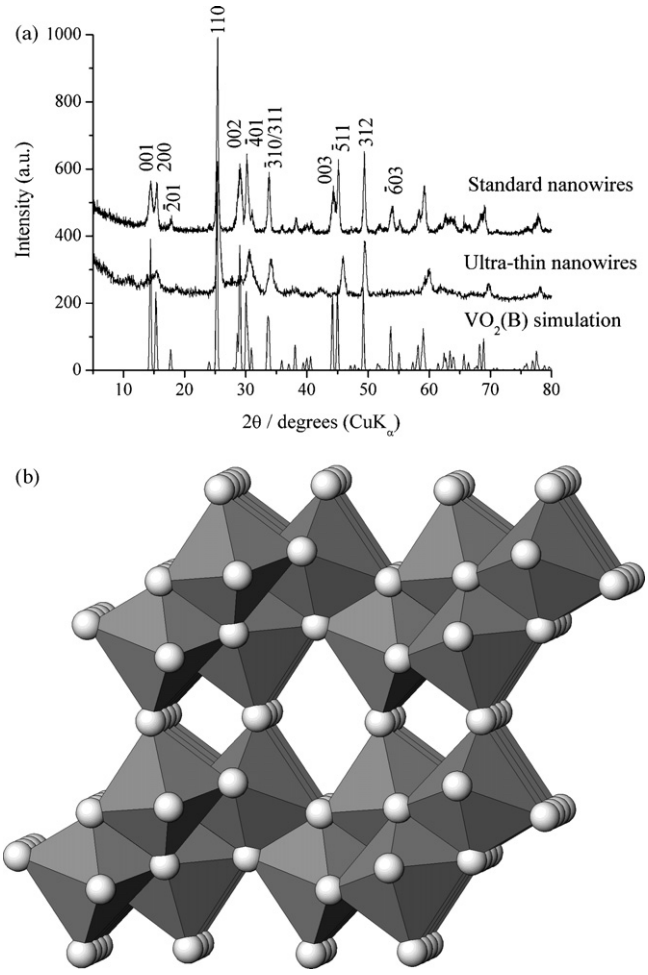

Fig. 3. (a) Powder XRD patterns comparing standard and ultra-thin VO_2(B) nanowires, together with a simulation for bulk VO_2(B). (b) Crystal structure of VO_2(B) viewed down *b*-axis. VO_6 octahedra: grey; O: white circles.

the reflections with a strong component along the [0 0 1] direction, e.g. (0 0 1), (0 0 2), (0 0 3) reflections as shown in Fig. 3a. This direction is perpendicular to the long axis of the wires and, especially given that these are arranged in bundles, severe preferred orientation is expected to be the origin of the missing peaks.

3.2. Electrochemistry

The nanowires were incorporated into composite electrodes, which were in turn assembled into cells as described in the Section 2. Previous studies of vanadium oxide electrodes in electrolytes containing DMC have indicated significant capacity fade associated with instability of the electrode in such electrolytes [34]. We confirmed that capacity fading occurs with VO_2(B) in cells containing LP30 electrolyte ($LiPF_6$ in EC/DMC (1:1, v/v)). In order to avoid this problem we employed a 1-m solution of $LiPF_6$ in PC as an electrolyte.

The charge–discharge curves for the first cycle of ultra-thin and standard VO_2(B) nanowires, collected at low rate, are shown in Fig. 4. The basic shapes of the load curves for the two sets of nanowires are similar, both exhibiting a

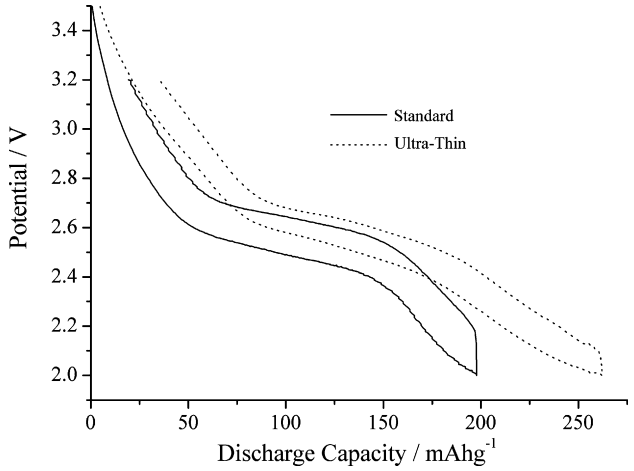

Fig. 4. Load curves of VO_2(B) nanowires at a rate of 10 mA g^{-1} in 1 M $LiPF_6$ in PC.

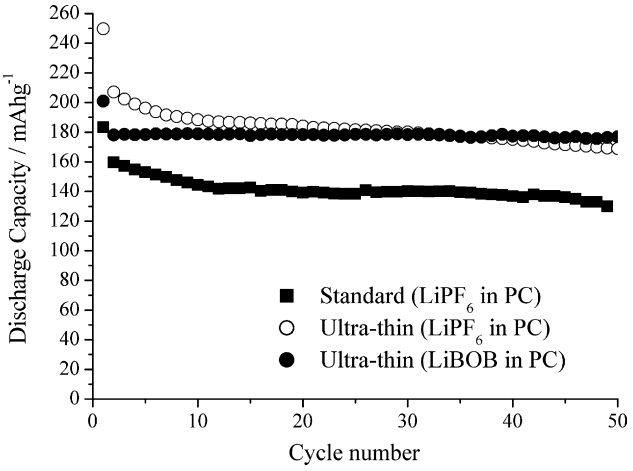

Fig. 6. Discharge capacity vs. cycle number for VO_2(B) nanowires at a rate of 50 mA g^{-1} in $LiPF_6$ in PC and LiBOB in PC, 2.0–3.2 V.

pseudo-plateau in the middle of the capacity range. However, the ultra-thin wires exhibit a higher discharge (intercalation) capacity (265 mAh g^{-1}) compared with the standard wires (200 mAh g^{-1}). Given that the separation of the charge and discharge curves for the ultra-thin wires is less than that for the standard wires, it is likely that this increased capacity corresponds to faster kinetics for the ultra-thin wires, resulting from their smaller diameter, which leads to shorter diffusion pathways for Li upon intercalation. It should also be noted that the range of solid solution, both before and after the pseudo-plateau, is greater for the ultra-thin wires. This may be a further demonstration of the fact that on reducing the dimensions of a material, the range of solid solution can increase, as shown recently for Li_xFePO_4 [5,35].

The evolution of the load curves for ultra-thin VO_2(B) nanowires on cycling is shown in Fig. 5. Some irreversible capacity loss is noted, but mainly on the first cycle, a feature often observed for intercalation compounds [6,16,18]. Aside from this small irreversible capacity loss on cycle 1, the shapes of the load curves remain relatively stable on cycling. Evolution of the capacity with cycle number is more clearly represented in Fig. 6, where it is compared with the standard VO_2(B) nanowires cycled under identical conditions. The first cycle capacity loss is again evident with a smaller degree of capacity fade continuing to occur over the first few cycles, thereafter capacity retention is good. Comparing these results with those for the standard wires, the latter also shows capacity fade on the first cycle, albeit of a somewhat lower magnitude, and capacity fade over the next few cycles, after which capacity retention is marginally better than the ultra-thin wires. Cycling was also carried out in a non-fluorinated electrolyte, 1 m solution of LiBOB in PC, in contact with the ultra-thin nanowires. Despite a lower initial capacity, there is negligible fade after the first cycle, suggesting that the slow fade observed for the $LiPF_6$-based electrolyte after cycle 1 may be due to reaction between the VO_2(B) and HF in the electrolyte. Overall, Fig. 6 emphasises the higher capacities obtained with the ultra-thin wires.

Given that the shape of the load curves for both ultra-thin and standard nanowires suggests the presence of two solid solution regions separated by a two-phase region, it is interesting to explore the structural changes that accompany lithium intercalation and deintercalation. Powder X-ray diffraction data collected on the standard nanowires as a function of the state-of-charge and on cycling are shown in Fig. 7. The standard nanowires

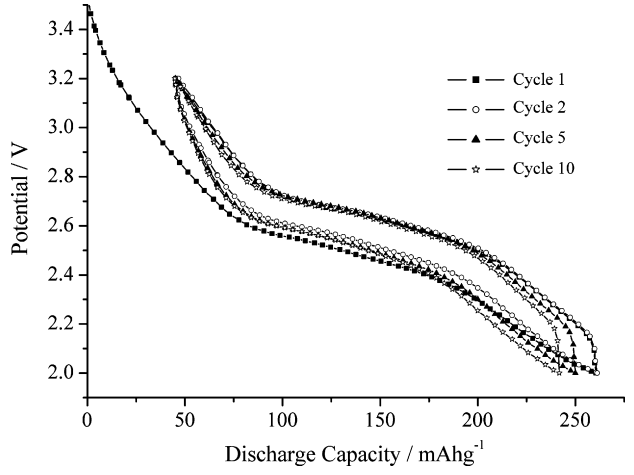

Fig. 5. Load curves of ultra-thin VO_2(B) nanowires at a rate of 50 mA g^{-1} in $LiPF_6$ in PC for several cycles.

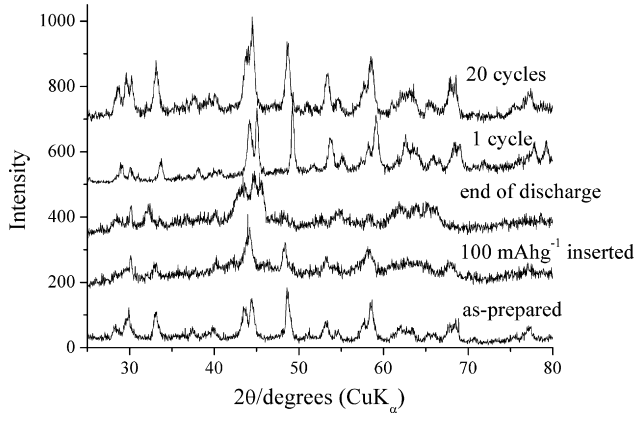

Fig. 7. Powder XRD patterns of standard VO_2(B) nanowires on cycling.

were chosen because they exhibit load curves with the same features as the ultra-thin wires but possess better quality powder diffraction data, permitting a more detailed interpretation of the structural evolution. Comparing first the powder X-ray diffraction pattern for the as-prepared wires with that for the wires at the end of discharge (corresponding to a lower cut-off potential of 2 V versus Li^+(1 M)/Li), it might appear at first sight that there has been a significant structural change on intercalation. However all of the peaks can be indexed on the same unit cell as the parent material, the changes in the powder diffraction pattern being explained by a significant expansion along the *b*-direction. Indeed, a similar powder diffraction pattern has been observed previously for a lithium intercalated bulk VO_2(B) for which the same interpretation was given [36]. There is no change of the gross structure on intercalation and the powder diffraction pattern for an electrode arrested on partial discharge (corresponding to 100 mAh g^{-1} of charge inserted) may also be indexed on the same VO_2(B) unit cell. The powder pattern after one complete cycle is very similar to the as-prepared material as is the pattern after 20 cycles. We can conclude that overall there are no gross structural changes occurring on lithium intercalation, deintercalation or cycling. TEM data collected for ultra-thin and standard VO_2(B) nanowires after 200 cycles are shown in Fig. 8. These data confirm retention of the morphology and demonstrate that cycling has not resulted in severe break-up of the ultra-fine nanowire bundles.

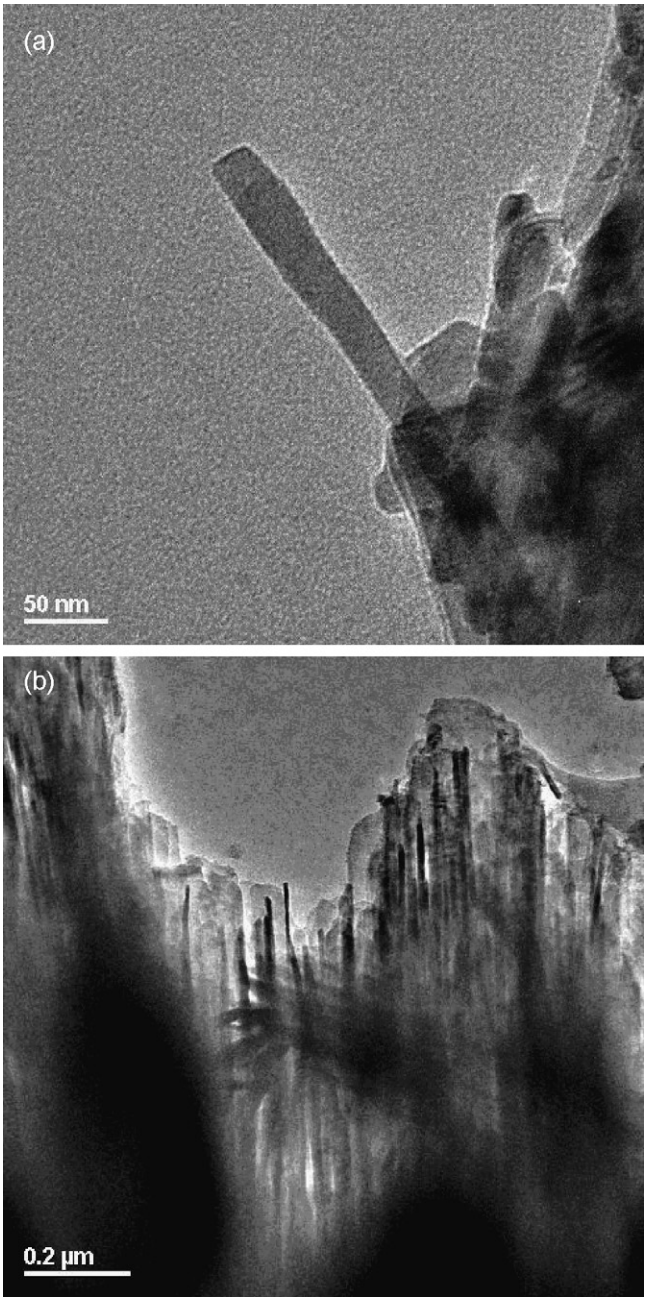

Fig. 8. Transmission electron micrographs for (a) standard VO_2(B) nanowires after 150 cycles and (b) ultra-thin VO_2(B) nanowires after 200 cycles.

The above results indicate that the shape of the load curves cannot be explained by any gross structural or morphological changes and therefore must arise from the more subtle effects. The weak scattering of X-rays by lithium leaves open the possibility that lithium ordering may occur within the basic VO_2(B) structure, leading to the pseudo-plateau behaviour observed in the load curves, however this will require further investigation by powder neutron diffraction, even then, given the width of the diffraction peaks anticipated as a result of the nanodimensions, it may prove difficult to obtain direct structural evidence for such ordering.

4. Conclusions

In conclusion, the synthesis, structural/morphological characterisation and electrochemical behaviour of ultra-thin (6–10 nm) VO_2(B) nanowires have been reported. Capacities of 265 mAh g^{-1} can be obtained from the ultra-thin wires and after some capacity loss on the first few cycles, good capacity retention is demonstrated on cycling. The ultra-thin wires deliver a higher capacity to store charge than the standard wires cycled under the same conditions (200 mAh g^{-1}). There is no evidence for gross structural or morphological changes during lithium intercalation, deintercalation and cycling.

Acknowledgement

PGB is indebted to the EPSRC for financial support.

References

[1] A.S. Aricò, P.G. Bruce, B. Scrosati, J.-M. Tarascon, W. van Schalkwijk, Nat. Mater. 4 (2005) 366.
[2] P.G. Bruce, B. Scrosati, J.-M. Tarascon, Angew Chem. Int. Ed., in press.
[3] P. Balaya, A.J. Bhattacharyya, J. Jamnik, Y.F. Zhukovskii, E.A. Kotomin, J. Maier, J. Power Sources 159 (2006) 171.
[4] A.D.W. Todd, R.A. Dunlap, J.R. Dahn, J. Alloys Compd. 443 (2007) 114.
[5] N. Meethong, H.Y.S. Huang, W.C. Carter, Y.M. Chiang, Electrochem. Solid State Lett. 10 (2007) A134.
[6] P. Reale, S. Panero, B. Scrosati, J. Garche, M. Wohlfahrt-Mehrens, M. Wachtler, J. Electrochem. Soc. 151 (2004) A2138.
[7] F. Jiao, P.G. Bruce, Adv. Mater. 19 (2007) 657.
[8] S. Nordlinder, L. Nyholm, T. Gustafsson, K. Edstrom, Chem. Mater. 18 (2006) 495.
[9] F. Jiao, K.M. Shaju, P.G. Bruce, Angew Chem. Int. 44 (2005) 6550.

[10] Y.K. Zhou, H.L. Li, J. Mater. Chem. 12 (2002) 681.
[11] B. Ellis, P.S. Herle, Y.H. Rho, L.F. Nazar, R. Dunlap, L.K. Perry, D.H. Ryan, Faraday Discuss. 134 (2007) 119.
[12] P.S. Herle, B. Ellis, N. Coombs, L.F. Nazar, Nat. Mater. 3 (2004) 147.
[13] L. Taberna, S. Mitra, P. Poizot, P. Simon, J.M. Tarascon, Nat. Mater. 5 (2006) 567.
[14] A.R. Armstrong, G. Armstrong, J. Canales, P.G. Bruce, Angew Chem. Int. Ed. 43 (2004) 2286.
[15] G. Armstrong, A.R. Armstrong, J. Canales, P.G. Bruce, J. Chem. Soc., Chem. Commun. (2005) 2454.
[16] A.R. Armstrong, G. Armstrong, J. Canales, R. García, P.G. Bruce, Adv. Mater. 17 (2005) 862.
[17] A.R. Armstrong, G. Armstrong, J. Canales, P.G. Bruce, J. Power Sources 146 (2005) 501.
[18] G. Armstrong, A.R. Armstrong, J. Canales, P.G. Bruce, Electrochem. Solid State Lett. 9 (2006) A139.
[19] F.J. Morin, Phys. Rev. Lett. 3 (1959) 34.
[20] F. Théobald, J. Less-Common Met. 53 (1977) 55.
[21] Y. Oka, T. Yao, N. Yamamoto, J. Mater. Chem. 1 (1991) 815.
[22] C. Tsang, A. Manthiram, J. Electrochem. Soc. 144 (1997) 520.
[23] A.M. Kannan, A. Manthiram, Solid State Ionics 159 (2003) 265.
[24] E. Baudrin, G. Sudant, D. Larcher, B. Dunn, J.M. Tarascon, Chem. Mater. 18 (2006) 4369.
[25] Z. Gui, R. Fan, W.Q. Mo, X.H. Chen, L. Yang, S.Y. Zhang, Y. Hu, Z.Z. Wang, W.C. Fan, Chem. Mater. 14 (2002) 5053.
[26] K.C. Kam, A.K. Cheetham, Mater. Res. Bull. 41 (2006) 1015.
[27] W. Chen, J.F. Peng, L.Q. Mai, H. Yu, Y.Y. Qi, Solid State Commun. 132 (2004) 513.
[28] X.Y. Chen, X. Wang, Z.H. Wang, J. Wan, J.W. Liu, Y.T. Qian, Nanotechnology 15 (2004) 1685.
[29] B.B. Li, X.M. Ni, F. Zhou, J. Cheng, H.G. Zheng, M.R. Ji, Solid State Sci. 8 (2006) 1168.
[30] S. Pavasupree, Y. Suzuki, A. Kitiyanan, S. Pivsa-Art, S. Yoshikawa, J. Solid State Chem. 178 (2005) 2152.
[31] G.C. Li, K. Chao, H.R. Peng, K.Z. Chen, Z.K. Zhang, Inorg. Chem. 46 (2007) 5787.
[32] A.R. Armstrong, P.G. Bruce, unpublished results.
[33] F.R. Theobald, R. Cabala, J. Bernard, J. Solid State Chem. 17 (1976) 431.
[34] F. Tanguy, J. Gaubicher, P. Soudan, N. Bourgeon-Martin, V. Mauchamp, D. Guyomard, Electrochem. Solid State Lett. 10 (2007) A184.
[35] A. Yamada, H. Koizumi, S.I. Nishimura, N. Sonoyama, R. Kanno, M. Yonemura, T. Nakamura, Y. Kobayashi, Nat. Mater. 5 (2006) 357.
[36] J.W. Jiang, J.R. Dahn, J. Electrochem. Soc. 153 (2006) A310.